

A Layer-by-Layer Quality Monitoring Framework for 3D Printing

Abstract

In this study, a layer-wise framework is proposed to monitor quality of 3D printing parts based on top-view images. The proposed statistical process monitoring method starts with self-start control charts that require only two successful initial prints. Answering the challenges of image processing due to lighting, a Machine Learning (ML) method is adopted to separate each layer from the printing bed. A sample image is compared to the standard image from a good part at each layer. The number of pixels in the difference images is fed into the proposed control charts to monitor printing process at each layer. An EWMA chart based on the number of pixels is used for process monitoring at each layer. Once enough parts have been printed, homogeneous layers are clustered to reduce the number of control charts needed for process monitoring. Experimental results based on a 3-inch diameter basket part show that the proposed framework is able of detecting various defected layer consistently.

Keywords

Quality Monitoring; Image Processing; Machine Learning, Self-Start Control Charts, EWMA

1. Introduction

The ability of Additive manufacturing (AM) generating parts with complex geometry makes it a viable manufacturing option. In recent years, many mainstream manufacturing industries such as aerospace, automotive, biotechnical/medical, and consumer products have adopted AM a part of their manufacturing strategy. ISO/ASTM 52900 defined AM as “a process of joining materials to make parts from 3D model data, usually layer upon layer, as opposed to subtractive manufacturing and formative manufacturing methodologies, ranks high on the transformative scale” (ISO and ASTM, 2015). In order to reach the full potential of AM, quality monitoring during a printing process is crucial to ensure production efficiency and customer satisfaction. However, most 3D printers are not equipped with an automatic quality monitor feature. The lack of supervision may result in wasted prints especially if the printing problems occurred in early layers (Farhad Imani , Bing Yao , Ruimin Chen , Prahalad Rao , Hui Yang, 2019). Machine

vision provides a mean for an automatic process monitoring operation. Automatic process monitoring is very important for large scale 3D printing operations in which hundreds of 3D printing machines are used in mass production of the same part. Even for small-batch 3D printing jobs, automatic process monitoring is also important in that there is not many printed parts for implementing traditional statistical process monitoring methods. A phase I control charting may not be established when the batch size is less than 20 parts.

SASAM drafted additive manufacturing roadmap and standards for quality and performance is one of the five high priority areas (SASAM, 2015; Chee Kai Chua, Chee How Wong and Wai Yee Yeong, 2017). Figure 1 shows 10 frequent cause for poor quality in 3D printing products. Some of those causes such as not initial setup issues could be done by analyzing images from printer bed with computer without involving human operators.

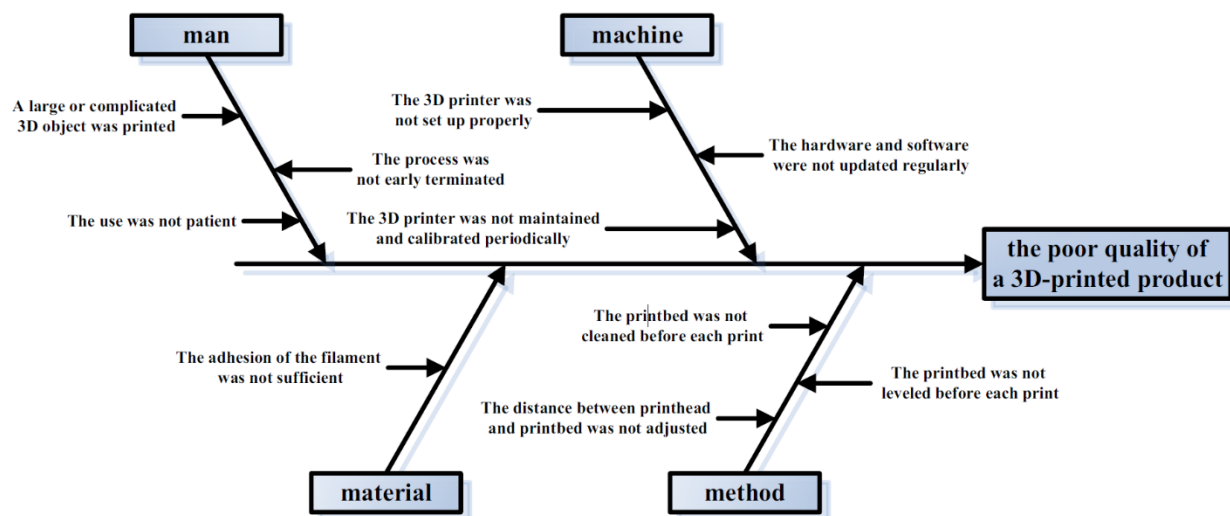


Figure 1. Fishbone diagram of the poor quality of a 3D-printed product (Hsin-Chieh Wu, Tin-Chih Toly Chen, 2018)

Due to the rich process information that can be captured, images and videos are increasingly deployed to monitor an AM process. Machine vision system (MVS) can be used to inspect quality characteristics in many different industries such as liquid crystal display, ceramic tiles, textile, and food products (Fadel M. Megahed, William H. Woodall & Jaime A. Camelio, 2011). Typically a MVS usually include a device to capture images (e.g. a vision sensor or cameras) and a computer to analyses and process the images captured by devices (Elias NMalamas, Euripides

G.M Petrakis, Michalis Zervakis, Laurent Petit, Jean-Didier Legat, 2003). MVSs have been increasingly used in industrial process monitoring due to the efficiency increasing and cost reduction (Zhen He, Ling Zuo, Min Zhanga, Fadel M. Megahed, 2016). However, high-dimensionality, correlation structure and complex data characteristics present many challenges for existing process monitoring methods to fully utilize the information of color images (Hao Yan, Kamran Paynabar, and Jianjun Shi, 2015). By integrating MVS and SPC in manufacturing process monitoring, not only product quality can be monitored, but also information gleaned from product images can be used for diagnostic analysis (Zhen He, Ling Zuo, Min Zhanga, Fadel M. Megahed, 2016; Xiaoxiao Guo, 2019).

In this study, an image-based quality monitoring framework is applied to 3D printing layer by layer. The proposed framework can be implemented to any 3D printed part. The proposed framework is illustrated by a 243-layer basket part with 3-inch diameter and 1.5-inch tall shown in Figure 2. An overhead camera takes image after a printer finishes each layer. The traditional SPC phase I process requires at least 20 to 25 parts to establish control limits and each layer requires one set of control charts. Since the material and resources using in 3D printing is usually expensive, the challenge is how to monitor the process from the very beginning when there is not enough samples to establish these control charts. Thus the proposed framework first relies on one self-start control chart on each layers after two successful prints are established. Then the homogeneous layers are clustered for families of control charts as more successful parts are acquired.

The rest of this paper is organized as follow. Section two provides some research background of imaged base quality monitoring with focus on additive manufacturing. The practical problem and experimental set up to collect data is presented in sections three and four, respectively. Section five are devoted to two subsections of image preprocessing and proposed process monitoring framework. Then an experimental example is presented to highlight how the proposed methodology can be applied to a real-world problem. Finally, conclusion and future research can be found in section seven.

2. Research background

A wide variety of quality characteristics such as product geometry, surface analysis, dimensional data, and defect patterns can be monitored using imaged based monitoring (Fadel M. Megahed, William H. Woodall & Jaime A. Camelio, 2011). Image-based quality monitoring includes the following steps: image acquisition, image pre-processing, feature extraction, and process monitoring, and control charts (Hao Yan, Kamran Paynabar, and Jianjun Shi, 2015). Previous research in this area mostly focused on two approaches (Zhen He, Ling Zuo, Min Zhanga, Fadel M. Megahed, 2016). The first approach uses spatial control chart to detect the location of and size of a defect (B. C. Jiang, C.-C. Wang, H.-C. Liu, 2005; Bernard C. Jiang, S.J. Jiang, 1998; Lu, C. J., and D. M. Tsai, 2005; Lin, H. D., and S. Chiu, 2006; Tunák, M., and A. Linka, 2008) while the second approach aims to detect defects through a well-defined statistical method (Armingol, J. M., J. Otamendi, A. de la Escalera, J. M. Pastor, and F. J. Rodriguez, 2003; Wang, K., and F. Tsung, 2005). These two approaches may be implemented simultaneously (Megahed, F. M., L. J. Wells, J. A. Camelio, and W. H. Woodall, 2012).

The idea of using control charts to monitor image data was first proposed by Hosrt and Negin (R.L. Horst, M. Negin, 1992) for dimensional control of web production processes. They showed that the use of control charts with image data improved productivity and profitability significantly. Koosha *et al.* (Mehdi Koosha, Rassoul Noorossana, Fadel Megahed, 2017) applied imaged-based SPC for nonparametric profile monitoring. They monitored coefficient of extracted features with a generalized likelihood ratio (GLR) control chart. Their results under different fault test showed that their model was able to detect shifts quickly.

Delli and Chang (Ugandhar Delli, ShingChang, 2018) proposed a SVM method to distinguish good parts from bad parts based on segments on printed images at critical checkpoints. Each image was first segmented into an 8 x 8 lattice forming 64 stamps. RGB statistics of these stamps were fed into the proposed SVM for a go/no-go determination. A major drawback of this method was that a large number of training images including both good and bad parts were required. Often time the bad parts were hard to collect and might take a long time before this proposed process monitoring method could be implemented.

Imani *et al.* (Farhad Imani, Aniruddha Gaikwad, Mohammad Montazeri, Prahalada Rao, Hui Yang, Edward Reutzel, 2018) used a layer-by-layer image analysis to detect the onset process

conditions that led to a lack of fusion-related porosity from in-process sensor data in laser powder bed fusion additive manufacturing. Their goal was not only to quantify size, number and location of pores but to identify process conditions that were liable to cause porosity through analysis of in-process, layer-by-layer images. They successfully examined and showed that several machine learning technics could be used to detect pores in laser additive manufacturing. Imani *et al.* (Farhad Imani, Ruimin Chen, Evan Diewald, Edward Reutzel, Hui Yang, 2019) implemented a deep learning neural network in layer-wise imaging profile for additive manufacturing quality control. In reality, there might be several layers of printing and quality features in 3D printing parts which could generate a large amount of data which was hard to track and monitor. Zou *et al.* proposed an EWMA and region growing based control chart to monitor images of production lines where the quality characteristic had either a specific pattern or uniformity character (Ling Zuo, Zhen He, Min Zhang, 2019).

The above-mentioned literature all requires sufficient amount of data for proper training. Most machine learning algorithms require a large amount of training data in each data category for satisfactory results. The number of sample images should be at least 20 to 25 for the Phase I process of traditional SPC charts (Montgomery, 2013). In addition, most of the previous research in imaged based quality monitoring assumes the statistic gleaned from the images are i.i.d. (i.e. independent and identically distributed), which may not be accurate. The main challenges are how to automate monitoring of in-process parts layer-by-layer using a limited amount initial image data.

Addressing these challenging issues using images for process monitoring, this study proposes a self-start and cluster-charting framework to monitor the print quality layer by layer from the third printing part using layer images. The process monitoring will start with a self-start control chart over layer-wise images in the beginning and switch to a cluster-charting approach after enough good parts are printed. The cluster-charting approach include an ARIMA filter to alleviate the autocorrelation of statistics from adjacent layers and then use one EWMA control chart for each homogenous layer family.

3. Problem Description Illustrated by a Case Study

In 3D printing industry, quality of 3D printed parts is checked when a part is printed. This practice means that if there is a mistake even in the first layer of printing, not only it can cause a significant waste in material and time but also the part should be printed again. Figure 3 (a) and (b) show two defect samples that can happen in a 3D printing process toward the end of a printing process. Figure 3 (c) shows another defect when operator discovered the problem at an early stage and stopped the printing process. This study attempts an automatic inspection framework to monitor quality of parts after each layer of printing by taking pictures and compare them with a standard print image. To do this, RGB values for each pixel in the image is compared to the same pixel location in the corresponding standard image. A gray-scale image can be represented as a function $f(x, y)$ where x and y can take non-negative integer values. For an 8-bit unsigned integer, this value is between 0 (black) and 255 (white) and the same color for a 16-bit unsigned integer is between 0 and 65535. However, printed layers are a small proportion of the printing bed as shown in Figure 2 and a small change in lightening may cause a large difference in RGB values.

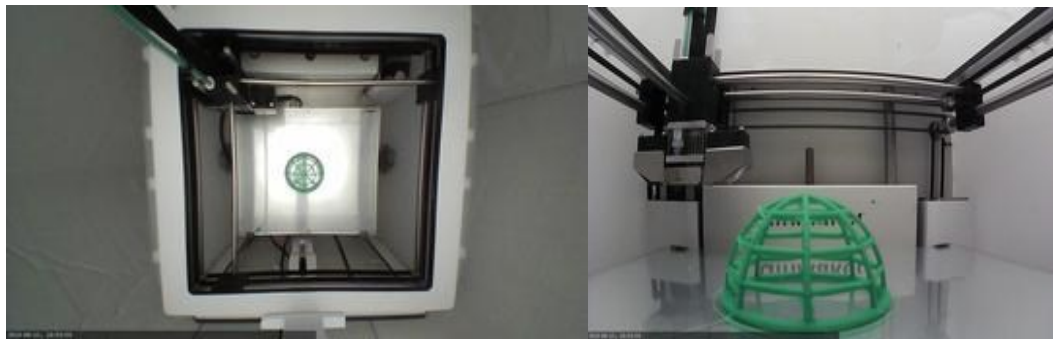


Figure 2. Experimental setup

To avoid this problem, the proposed method first classifies each pixel into two classes: a part of the print or not a part of the print. This way, the part image is isolated from the machine bed and its environment so just the parts would be compared and not the environment. Then the filtered image containing only the part can be compared to a standard image. Two quality monitoring techniques in the proposed framework are then applied on the difference of sample and standard images to determine whether the process is in control or not.

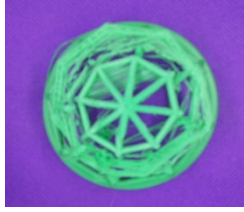


Figure 3. (a) Defect at the end of process



(b) Toward final layers of printing



(c) Defect during early stage of printing

4. Proposed Method

The proposed method contains two major steps. The first step is image classification where images will be cleaned, prepared and processed. The second is the process monitoring based on the processed images. Figure 4 shows the proposed imaged-based quality monitoring framework. This framework starts with self-start control chart approach. In this approach in order to find inverse normal distribution (U_{nj}) at least two printed sample is needed. After printing two standard parts, the proposed framework will start by feeding image of first layer to monitor quality of the process. The basic assumption is that the quality of the two printed part is satisfactory. This process will be implemented for each layer of printing separately. Each step is explained in more details.

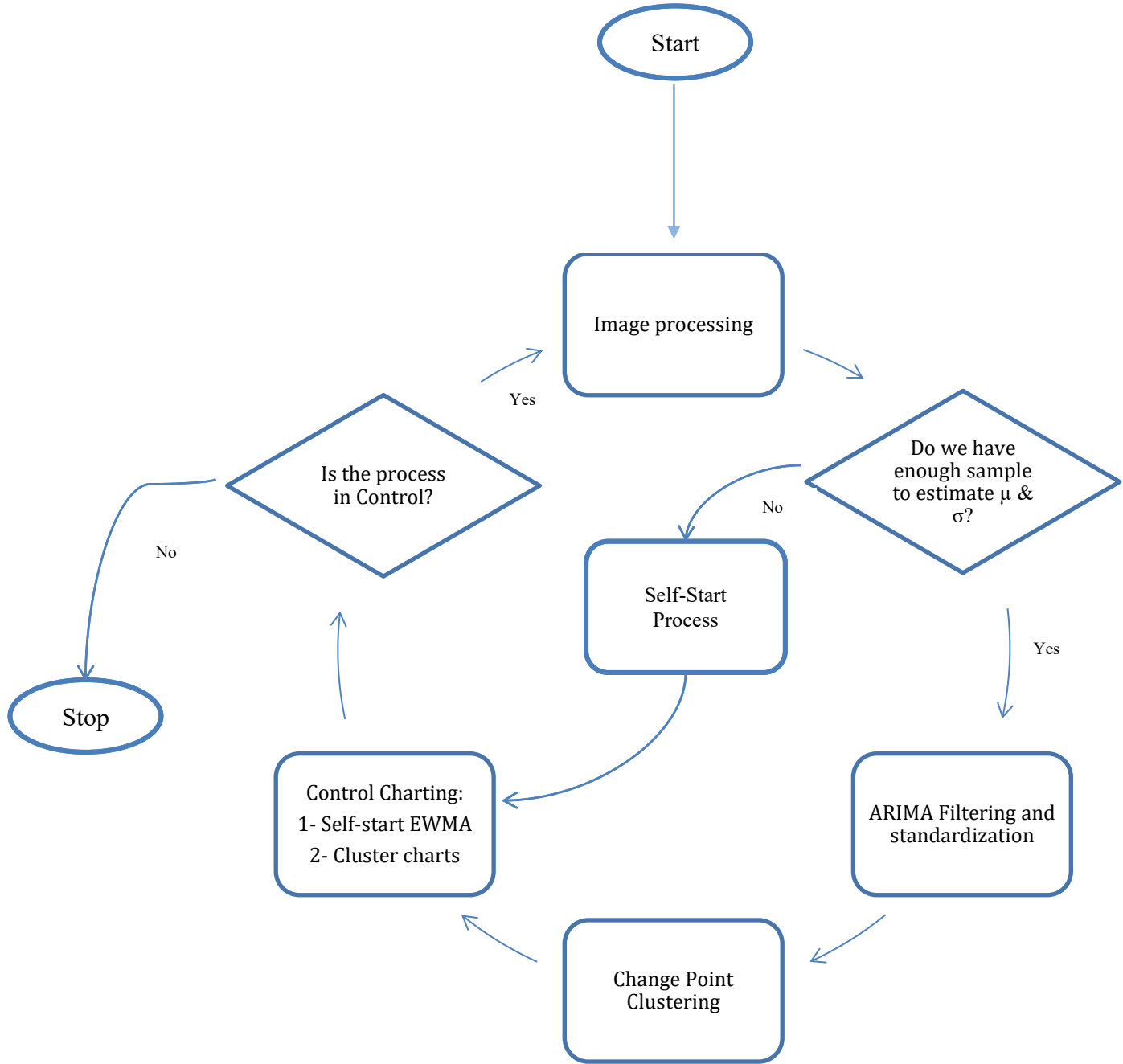


Figure 4. Layer-by-Layer Image-Based Quality Monitoring Framework for in-process 3D Printing Parts

4.1. Image Processing

Image processing is the first core stage in the proposed quality monitoring framework. Three major steps in this stage include image capturing, image filtering, and finally image extraction.

4.1.1. Experimental Setup and Image Capturing

The 3D printer used in this study was Ultimaker 3. Ultimaker Cura was used to design the part and to handle the G code, remote access to the camera feed, and take webcam snapshots. Octoprint software served as the operation platform was used to print a part and collect part images layer by layer. Figure 5 shows that the part design on Ultimaker Cura. Octoprint can be implemented in either on a PC or Raspberry Pi. To ensure consistent lighting, an enclosure was built to cover the Ultimaker printer. A strip lighting and a photography umbrella are mounted on the top of the enclosure. After printing of each layer, the G code instructed the printing head to its default location at the upper left-hand corner shown in the top view picture in Figure 2. Then the overhead webcam takes a picture. The material used for this research was PLA. The same 3D printer configuration was used throughout this study. Finally, Python 3.7 has been used for image processing and extraction.

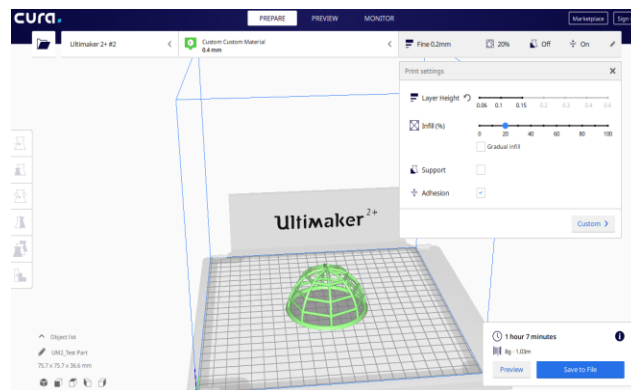


Figure 5. The part designed using Ultimaker Cura

Images were taken by two cameras – from the top (Figure 2 (a)) and from the front (Figure 2(b)) of the Ultimaker printer. In this paper we focus on the data only from top view camera. Side view images can be processed and analyzed using the same methods. In addition, we are working on using several cameras from the corners so that the printer head does not have to travel to the default location after each print. Figure 5 presents a possible angle for this implementation.

4.1.2. Image Pre-processing and Filtering

To make sure suitable images are generated with pixels containing part only, it is essential to clean the data. First, the portion containing the part in Figure 2(a) was cropped to contain only the printed layer and its surrounding bed area. Then the all pixels in the cropped image need to be classified into two classes: part only and printer bed. Finally, each pixel containing the RGB values is transformed from colored images into binary images with “part” and “not part” label. In other words, the proposed approach first converts the RGB values in each pixel into a gray scale value. Then a gray scale cut-off threshold value can be used for the binary classification task (Andres Patrignania, Tyson E. Ochsner, 2015). However, lighting is a significant issue as shown in Figure 6 where the reflection of the part on the printer bed causes some of the printer-bed pixels to be classified as a part of the part. A single threshold value cannot be implemented for the classification task.

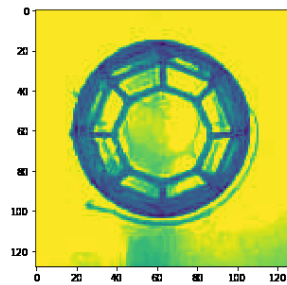


Figure 6. RGB to gray scale using skimage package on python

To overcome this issue, three different machine learning algorithms of Neural Network (NN), Gradient Boosting Classifier (GBC) and Support Vector Machine (SVM) from sklearn package in python were used to achieve the classification task. These methods were chosen because of their performance in binary classifications. NN and SVM are two well-known machine learning algorithm in binary classification and GBC is a newer and improved method based on random forest. Among three machine learning methods studied, SVM which had the worst performance while NN and GBC performed more than 90 percent accuracy. NN had slightly better performance than GBC in terms of (True Positive Rate (TPR) and False Positive Rate (FPR)), but GBC had lower FPR which is more critical to eliminate the part reflection on the printer bed

mistaken as the part in Figure 6. So in this research, GBC is chosen for further analysis. Figure 7 shows the AUC curves of the different ML methods studied. Comparing various ML methods we prefer AUC curves trending toward upper left-hand corner. The preliminary data shows that NN and GBC are capable of detecting part with 95 and 93 percent accuracy while SVM can only achieve 60 percent accuracy for pixel classification.

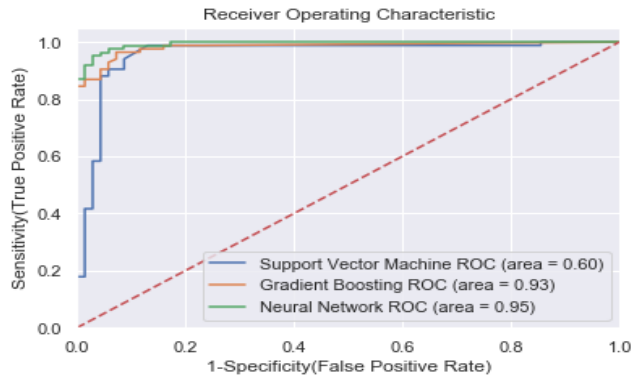


Figure 7. ML Performance Sensitivity vs

The GBC method was used for pixels classification. This process has to be done for all the layers in every single part. The sample part in this study has 243 layers. Figure 8 depicts the outcome for layer 200 of the first part. Figure 8(b) is the color image while 8(a) is binary image where the light color (i.e. yellow) represents “part” and the dark color (i.e. purple) is the printer bed. Due to the classification errors, the filtered image contains noise and loses resolution. As shown in the outer rim in the original image almost disappears in the filtered image. This sacrifice is necessary in that each pixel contains three values in Red, Green, and Blue, which cannot be directly used in the next stage of the proposed method, which is the image difference operation.

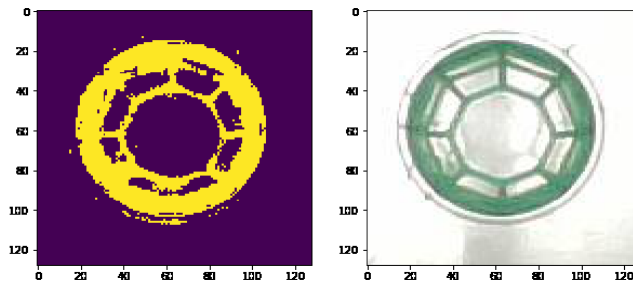


Figure 8. (a) GBC binary prediction on the left and (b) the actual part (Layer 200) on the right

4.1.3 Image Extraction

The outcome in the previous section is a gray-scale filtered image free of noise from lighting and background as shown in Figure 8(a). The proposed imaged-based process monitoring framework involves a layer-by-layer monitoring scheme. Specifically, any future sample layer would be compared to a good layer, which can be established when the first two good print is obtained. Each grayscale image from a given layer is represented in a two-dimensional matrix and resolution of each image is 128 x 128 in this case. To compare images, the 2D grayscale matrix of the sample layer should be subtracted from that of the first good layer. The pixels not containing any part (i.e. the printer bed) are already assigned the value zero by the proposed GBC algorithm in the last section while pixels containing the part are assigned the value 255. Consider the case of n parts each with m layers. Let M_{ij} be the image matrix, $i=1,2,\dots, n$ and $j=1,2, \dots, m$ and its resolution is 128x128. The element in the M matrix can be presented as $M(h, v)$ where horizontal index $h=1,2,\dots, 128$ and vertical index of $v=1,2, \dots, 128$. For example, M_{1j} is the image of the first part at j th layer. Define D_{ij} as the total number of different pixels for the j th layer between i th part and the first standard or good part.

Thus:

$$D_{ij} = \sum_{h=1}^{128} \sum_{v=1}^{128} \frac{|M_{ij}(h,v) - M_{1j}(h,v)|}{255} \quad \text{where } i=2, 3, \dots, n \text{ and } j=1, 2, \dots, m, h=v= 1, 2, \dots, 128. \quad (1)$$

Remember that M_{ij} is a matrix containing elements with zeros representing “no part” and 255 representing “part.” Thus the expression “ $M_{ij}(h, v) - M_{1j}(h, v)$ ” is a value of either 0 or a multiple of 255. When an element in D_{ij} is 255, it means that there is a difference in the sample image pixel and that of the first part at layer j . To find total different pixels we need to divide it by 255 and tally all elements in the matrix M_{ij} .

4.2 Process Monitoring

D_{ij} generated in equation (1) can be used for the process monitoring purposes. The goal of process monitoring is to ensure print quality at each layer as oppose to at the end of an entire part. Two complementary approaches are explored to monitor the production process depending on the amount of information available for Phase I of control charting. Traditional Phase I

control charting guideline demands at least 20 to 25 observations to establish a control chart. However, Hawkins [30] suggests the use of a self-start control charting procedure when this number can be reached. The first method applies one self-start control chart to each layer. The proposed approach can start from the third part after two parts are successfully printed and the layer-by-layer images are stored. Equation (1) is implemented to generate the statistic for control charting. Since the part in this study contains 243 layers, we use 243 control charts each for a layer. The second approach can be implemented when enough homogeneous sample statistics are available. The core idea is to use as fewer control charts as much as possible by grouping adjacent layers. Instead of using one control chart for each layer, statistics from “similar” layers can be plotted on the same control chart. This requirement can be met after multiple parts are successfully printed and similar adjacent layers can be clustered according to the distribution of the standardized D_{ij} . The one control chart is applied to each homogeneous cluster.

4.2.1 Method I: Self-start Charting

A self-start control chart can be used for process monitoring on the number of different pixels in the matrix D_{ij} , $j=1,2,\dots, m$. Hawkins (HAWKINS, 1987) proposed self-start Cumulative Sum Control Chart (CUSUM). In their proposed method, any other control charts can be applied when standardized values for observation is calculated. CUSUM is an approach to catch small shifts. However in image-based quality monitoring we are mostly interested to catch medium to large size shifts. Thus EWMA would be a better approach than CUSUM.

In this research we propose an EWMA self-start control chart to start monitoring of each layer from the third part. One control chart is applied for each layer of printing in this method and each point in the chart represents the quality at end of each layer. If the difference statistic D_{ij} plots within the control limits, it means that the process is in control. We could have chosen Individual X control chart in this case since the processing monitoring task is mainly for various mis-printing situations such as those in Figure 3(a)-(c). However, an IX chart requires the underly statistics are normally distributed which is not true in this case.

Equations for this method are summarized as follow where \bar{D}_{nj} is the average of the first n observations of D_{ij} and ω_{nj} the sum of squared deviations from \bar{D}_{nj} for each layer j :

$$\omega_{nj} = \sum_{i=1}^n (D_{ij} - \bar{D}_{nj})^2 \quad (2)$$

$$\bar{D}_{nj} = \bar{D}_{(n-1)j} + \frac{D_{ij} - \bar{D}_{(n-1)j}}{n} \quad (3)$$

Thus, we can have:

$$\omega_{nj} = \omega_{(n-1)j} + \frac{(n-1)(D_{ij} - \bar{D}_{(n-1)j})^2}{n} \quad (4)$$

The sample variance of first n observation (s_{nj}^2), standardized observation (T_{nj}), cumulative t distribution of standardized observation ($F_{(n-2)j}(a_{nj}T_{nj})$), and the transformation of inverse normal distribution (U_{nj}) formula for $n \geq 3$ are given as follow:

$$s_{nj}^2 = \frac{\omega_{nj}}{n-1} \quad (5)$$

$$T_{nj} = \frac{D_{ij} - \bar{D}_{(n-1)j}}{s_{(n-1)j}} \quad (6)$$

$$\text{Let } a_{nj} = \sqrt{\frac{n-1}{n}} \quad (7)$$

$$P(T_{nj} \leq t_j) = F_{(n-2)j}(a_{nj}T_{nj}) = F_{(n-2)j}\left(t_j \sqrt{\frac{n-1}{n}}\right) \quad (8)$$

$$U_{nj} = \Phi^{-1}[F_{(n-2)j}(a_{nj}T_{nj})] \quad (9)$$

Note that we assumed T_{nj} is normally distributed. A large value of D_{ij} means that huge difference between the printing part and first standard sample at layer j and a small number means the process is in control. So one can use values of U_{nj} in a CUSUM chart because in self-start we want to be careful about small and medium size changes. However, because of the lightening and environmental changes issues, and philosophy of CUSUM in catching very small changes, CUSUM for images-based quality monitoring might cause many false alarms. Thus we recommend the use of EWMA control charts for each layer j which is a better approach to catch medium to large size shifts by adjusting the EWMA parameter λ toward 1. Table 1 shows a self-start procedure calculation for layer 122 of our printed parts and Figure 9 demonstrate self-start EWMA control chart for layer 122 of first 16 parts.

Table 1. Self-Start control chart calculation for layer 122 of the first 16 parts

Part number(n)	D_{n122}	\bar{D}_{n122}	ω_{n122}	S_{n122}	T_{n122}	$a_{n122}T_{n122}$	$F_{(n-2)122}(a_{n122}T_{n122})$	U_{n122}
1	347	347	0	-	-	-	-	-
2	272	309.5	2812.5	53.03301	-	-	-	-
3	266	295	4074	45.13314	-0.82024	-0.66973	0.312159661	-0.48974
4	246	282.75	5874.75	44.25212	-1.08568	-0.94022	0.223177095	-0.76151
5	242	274.6	7203.2	42.43583	-0.92086	-0.82364	0.235258149	-0.72164
6	311	280.6667	8307.333	40.76109	0.857766	0.783029	0.761313095	0.710533
7	228	273.1429	10684.86	42.19964	-1.29208	-1.19624	0.142615765	-1.06864
8	319	278.875	12524.88	42.29974	1.086671	1.016488	0.82569006	0.93727
9	275	278.4444	12538.22	39.58886	-0.09161	-0.08637	0.466795854	-0.08333
10	404	291	26726	54.49363	3.171487	3.008737	0.991577035	2.390053
11	446	305.0909	48566.91	69.68996	2.844369	2.712	0.988040471	2.258427
12	418	314.5	60253	74.01044	1.620163	1.551188	0.924048633	1.432843
13	398	326.6154	82735.54	83.0339	2.128078	2.044591	0.967208136	1.841258
14	403	303.2857	179319.1	117.4469	-3.93352	-3.79043	0.001287113	-3.01448
15	400	283.0667	263557.7	137.2062	-2.58232	-2.49476	0.013426394	-2.21365
16	472	290.25	274343.3	135.2389	0.837668	0.811069	0.784550315	0.787654

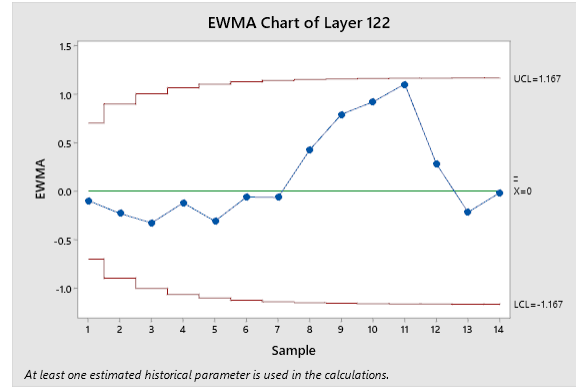


Figure 9. Self-start EWMA control chart for layer 122 of first 16 parts

4.2.2 Method II: Cluster Charting: Standardizing, Autocorrelation Filtering, Change Point Clustering

This cluster-charting method aims to reduce the number of control charts required in the self-start-charting method. Chang *et. al.* (Shing I.Chang, BehnamTavakkol, Shih-HsiungChou, Tzong-RuTsai, 2014) proposed a real-time detection of condensation-water-temperature wave

profile monitoring. The core idea is to monitor product quality during the curing process rather than at the end of the process. The same idea can be used in this application as well since 3D printing is accomplished layer by layer. Each layer represents a critical stage in the production process of interest. The print quality monitoring should take place at the end of each layer rather than at the end of the entire print. This method contains two major steps of standardization and ARIMA filtering and then change point clustering. Unlike the self-start control charting in section 5.1, we use much few charts for process monitoring.

5.2.2.1 Standardization and ARIMA filtering

The statistics in self-start control charts are independent because each point in a control chart comes from a different part. However, in the effort to plot statistics from different layers of the same part on the same control chart, the independent assumption may be violated. To test the i.i.d. assumption, we need to first standardize statistics D_{ij} .

$$e_{ij} = \frac{D_{ij} - \mu_j}{\sigma_j} \quad (10)$$

Note that in the self-start charting, control chart points are from different parts, i.e. $i=1,2, \dots$. The plot statistics are independent since they from different parts. In the cluster charting method, we want to use the same chart family to plot e_{ij} , $j=1,2, \dots$. The e_{ij} statistics, $j=1,2,\dots,m$, on the other hand, might be autocorrelated. Autocorrelation function plot (ACF) and Partial Autocorrelation function plot (PACF) can be used to test this autocorrelation. In order to remove the autocorrelation from e_{ij} we needed to apply a filter as in Figure 4. ARIMA can be used to remove autocorrelation from e_{ij} . If ACF dies out gradually and PACF cuts off sharply after a few lags then an AR filter is recommended and if PACF dies out gradually and ACF cuts off sharply then MA filter is recommended. After the filtering operation, the uncorrelated is named e'_{ij} .

4.2.2.2 Change Point Clustering

From the previous section, we have removed autocorrelation from the statistics and generated statistics e'_{ij} which come from different layers of the different sample part. The next step is to

cluster homogeneous streams of e'_{ij} for control chart families. Sullivan's change-point detection approach (Sullivan, 2002) is proposed for this task. This clustering algorithm for each part i find distance (d_{ik}) with $m - 1$ boundaries (k_j) which separating the layers into clusters:

$$\bar{x}_{ik} = \frac{\sum_{j=1}^k e'_{ij}}{k} \quad (11)$$

$$d_{ik} = \frac{|\bar{x}_{ik} - \bar{x}_{i(k+1)}|}{s_i \sqrt{\frac{m_{ik} + m_{i(k+1)}}{m_{ik} m_{i(k+1)}}}} \quad i = 1, 2, \dots, n, k = 1, 2, \dots, K \quad (12)$$

Where m_{ik} and number of layers in the adjacent clusters, s_i is an estimation of standard deviation of all clusters. Since the ranking of d_{ik} does not depend on the standard deviation so we can set it to one without loss of generality and \bar{x}_{ik} is the layers mean. Different parts might have different change points. In a typical 3D printing part, the difference from layer to layer may be very small. The implementation in the proposed self-start approach may be relaxed to allow adjacent layers to be combined. However, small incremental changes may accumulate to a large change.

Therefore, it is necessary to cluster similar layers in term of the statistic e'_{ij} together. This procedure can simply done by finding high density of change point around a specific layer. For example if most of the parts exhibit their first change point between layer 57 to 62 then probably layer 60 can be a general change point for all the parts. Note that the number of change points might be different from part to part. Therefore, we pick the maximum number of change points among all parts to this procedure. This practice might require more control charts but the number of charts is far less than the number of layers.

4.3 Control Charting

By having values of U_{nj} in the first method (self-start charting) and e'_{ij} in the second method, we propose to use method I to start process monitoring after two acceptable prints are accomplished. After more successful parts have been printed, we will switch to method II. Since each printing part has different characteristics, the timing and criteria for switching depends on how fast the estimates of μ_i and σ_i in equation (10) is stabilized.

In our problem we are mainly interested in catching medium to large shifts. EWMA control charts can be adjusted to meet these needs. Thus, in this case of self-start charting, EWMA control charts is used to plot U_{nj} . Each layer will be monitored with a control chart so 243

control charts will monitor the process. Self-start statistics are updated after every new printed layer. Same as the self-start charting, EWMA control charts can be used for each cluster. Note that estimation for standard deviation can be find by using $\frac{\overline{MR}}{d_2}$ where the \overline{MR} is the average of moving range from part to part for a layer and d_2 is a function of sample size. Since adjacent layers are used, e_{ij} of adjacent layer are used to estimate the standard deviation, $d_2=1.128$.

5. Numerical Results and Discussion

The proposed framework adopts various methods such as machine learning techniques, ARIMA filtering, self-start control charting, and change-points-detection for clustering for image-based monitoring of 3D printing parts. It aims to automatically detect bad prints in every layer using the proposed self-start control chart which only requires the first two successful prints. In this study, we printed 15 non-defect part plus a few defect parts to demonstrate the proposed methods.

5.1 Self-Start EWMA Control Charts

Self-start EWMA control charts have been designed to monitor the production process after printing two parts. In addition to the 15 non-defect parts that we already used to design the traditional EWMA control chart and to see performance of the method, a 16th defect part has been added to the data set. Figure 10(a) and (b) shows layer 122 and 123 of part 16 respectively. With a naked eye it looks there is no difference between two images. If an operator checked the process after each layer, he might not be able to understand if one extra layer is printed or not. However, layer 123 is the start point of making a defect part. It is might not be clear from these images but after layer 122, the part had a small shift on the bed and that small displacement cause the huge mess which can be seen in Figure 10 (c) as the last layer of this part.

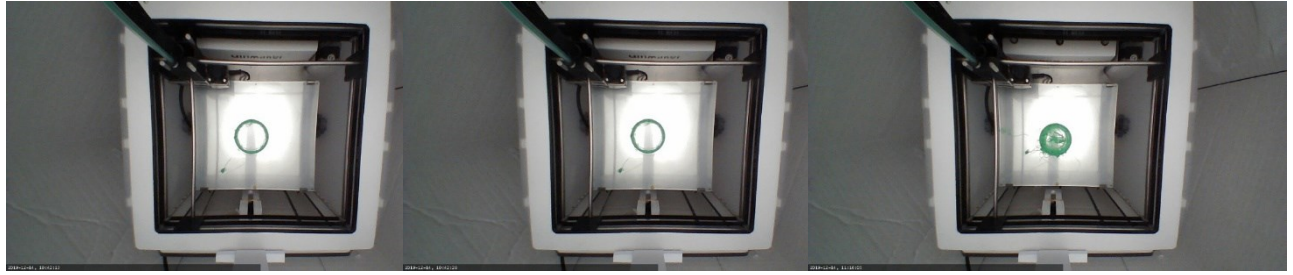


Figure 10. (a) Layer 122 of the 16th part (b) Layer 123 of the 16th part(c) Layer 243 of the 16th part

We already have seen self-start procedure for layer 122 of first 16 parts. To see how the proposed method catch this problem, we only need to run self-start EWMA control chart for layers 123. Table 2 shows self-start procedure calculation for layer 123

Table 2. Self-Start control chart calculation for layer 122 of the first 16 parts

Part number(n)	D_{n123}	\bar{D}_{n123}	ω_{n123}	S_{n123}	T_{n123}	$a_{n123}T_{n123}$	$F_{(n-2)123}(a_{n123}T_{n123})$	U_{n123}
1	322	322	0	-	-	-	-	-
2	275	298.5	1104.5	33.23402	-	-	-	-
3	293	296.6667	1124.667	23.71357	-0.16549	-0.13512	0.457247472	-0.10737
4	257	286.75	2304.75	27.71732	-1.67274	-1.44864	0.142221342	-1.07039
5	228	275	5066	35.58792	-2.11961	-1.89584	0.077131518	-1.42463
6	337	285.3333	8269.333	40.66776	1.742164	1.590371	0.906520918	1.319631
7	288	285.7143	8275.429	37.13809	0.065572	0.060708	0.523028147	0.057755
8	314	289.25	8975.5	35.80802	0.761636	0.712445	0.748530168	0.669872
9	283	288.5556	9010.222	33.56006	-0.17454	-0.16456	0.436970827	-0.15865
10	411	300.8	22503.6	50.004	3.648517	3.461287	0.995724206	2.629479
11	416	311.2727	34568.18	58.79471	2.303816	2.196602	0.972175973	1.913782
12	407	319.25	42968.25	62.49964	1.628161	1.558846	0.924954116	1.439207
13	390	324.6923	47581.52	62.96925	1.132007	1.087597	0.849985287	1.03637
14	419	331.4286	52574.35	63.59387	1.497678	1.443199	0.912721246	1.357704
15	411	336.7333	55816.25	63.14171	1.251244	1.208816	0.875869425	1.154583
16	1074	382.8125	532129.7	188.3489	11.67638	11.30561	0.99999999	5.611786

Even before plotting a control chart we can see a huge difference in the value of $U_{16, 123}$, but the EWMA control charts which has been presented in Figure 11 shows this issue even better. Note

that the standard deviation for the EWMA chart has been calculated with $\frac{\overline{MR}}{d_2}$ where the moving range is within a part among layers.

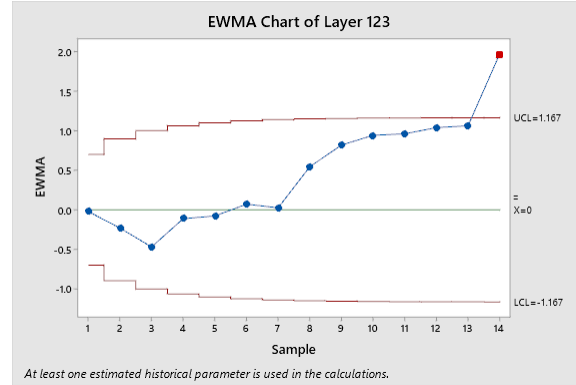


Figure 11. Self-start EWMA control chart for layer 123 of first 16 parts

Lightening issues and production environment changes makes some differences between same layers of different parts. Thus trends might not have a meaning of being out of control. Also, in this method we are not looking for catching small changes in the images. So, methods like CUSUM which is basically designed to catch small shifts might not be the best method to use due to the concern of false alarms.

5.2 Standardizing, ARIMA Filtering, Change Point Clustering

The case study of printed parts showed sufficient performance of self-start control charts in catching shifts from images data. However, monitoring the process using this approach carries a high overhead cost since there is one control chart for each layer or in this case 243 charts). Thus, Method II can be used to monitor each part based on printed layers of same part when we printed enough parts to estimate mean and variance.

Different approaches have been explored to find optimal number of observation to design control chart. However, traditionally it is recommended at least 20-25 observation is needed to do that (Montgomery, 2013). In Imaged base quality monitoring definition of observation might be different because there is one observation for each layer and layers from one part can be divided into different clusters. Finding sufficient number of observations to start this approach is

explained better in section 6.2.2. When there is enough samples to normalizing the data from D_{ij} to e_{ij} , we need to check the independent assumption. Figure 12 shows autocorrelation (ACF) and partial autocorrelation (PACF) on e_{ij} of part 11 as an example which shows images (especially in first layers) are highly autocorrelated. They suggest that the underlying autocorrelated structure may be modeled by an autoregressive model.

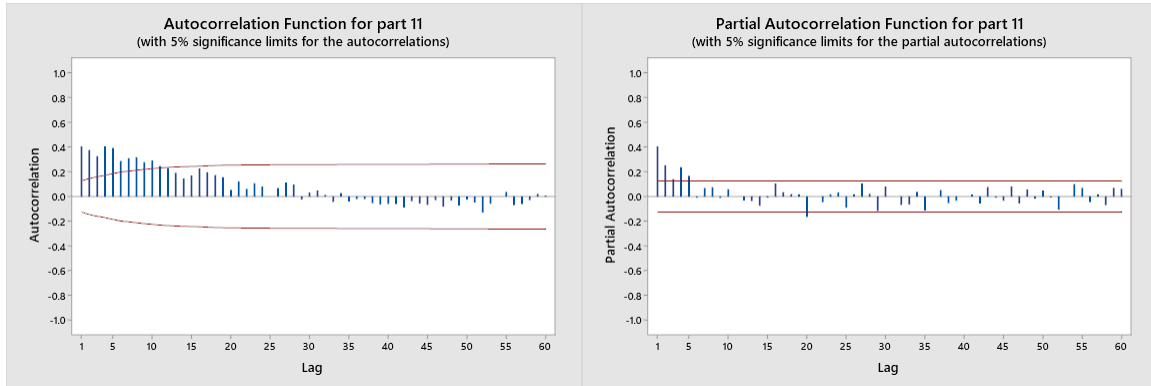


Figure 12. ACF and PCF of part 11

5.2.1 ARIMA Filter

According to the PACF and ACF in Figure 12 we can see there are two spikes in the PACF so we can conclude the best type of filter to remove autocorrelation would be AR(2). After applying AR(2) over e_{ij} , the uncorrelated variable is named e'_{ij} . Figure 13 shows uncorrelated ACF after applying AR(2).

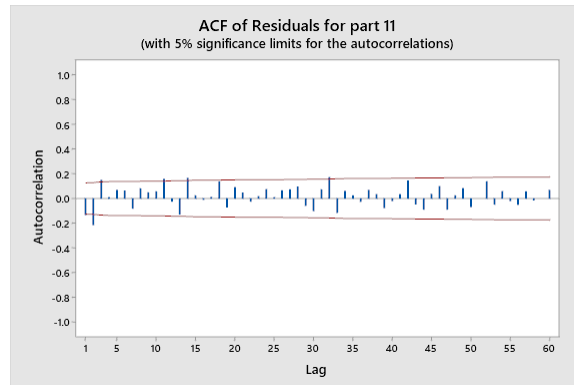


Figure 13. Autocorrelation (ACF) of part 11 after applying AR(2)

5.2.2 Change point segmentation

Next step is finding change points. To do this we can plot change point detection method proposed by Sullivan (Sullivan, 2002) for each part separately. However, in phase I of quality monitoring, we need to design our process and control limits and having different change point for different part could be a problem and is not efficient. Figure 14 shows time series plot of part 11 and Figure 15 shows time series plot of location and distance for the same part. By comparing change point of all 15 parts we conclude that for most of parts, one change happens between layer 59-63 and another between layers 185-195. Thus the best segmentation looks to be (1, 60), (61, 180), (181, 243). Part 11 was chosen to demonstrate process monitoring with this method because of three clusters of layers. As we mentioned before, usually 20-25 observation is needed to design Shewhart control chart. In this case, since three charts are used and each chart has more than 60 observation (layers), thus 10 parts should be enough to estimate mean and variance. Thus, we can switch from the Method I self-start charting to Method II cluster-charting starting from part 11.

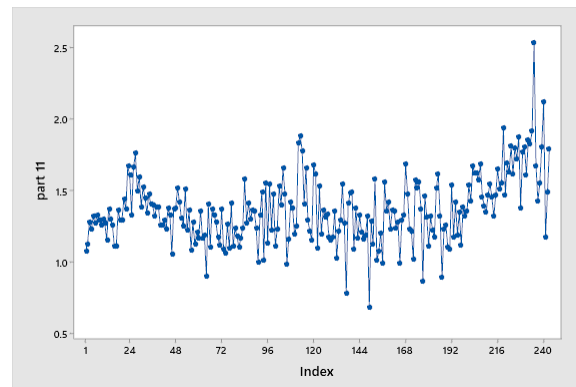


Figure 14. Time series plot of e'_{ij} of part 11

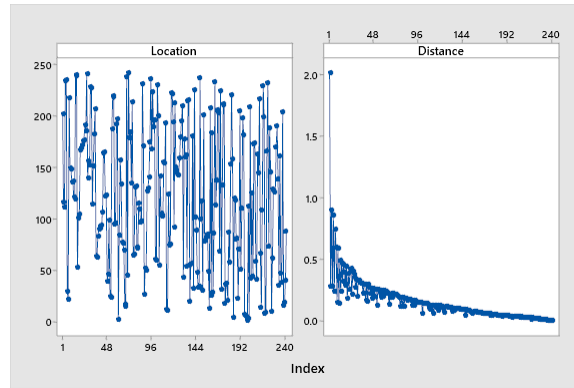


Figure 15. Time series plot of location, and distance for part 11

In the next (and final) step of this method, a EWMA control chart is plotted for each cluster of layers. Figure 16 (a), (b), and (c) shows the control chart for layers 1-60, 61-180, and 180-243 respectively.

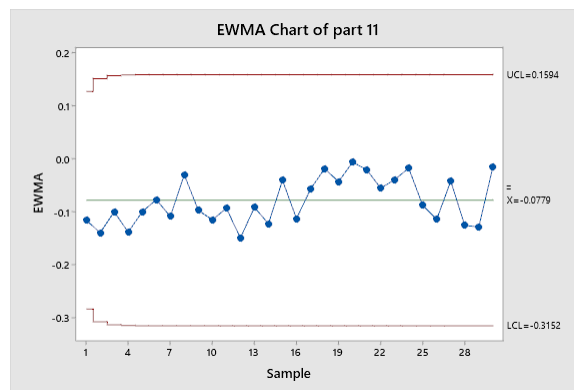


Figure 16. (a) EWMA control chart for layers 1-60 part 11

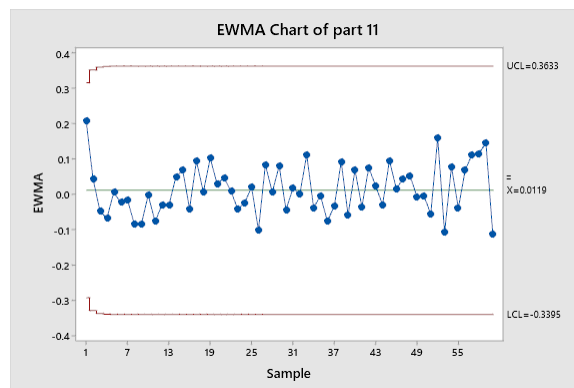


Figure 16 (b) EWMA control chart for layers 61-180 part 11

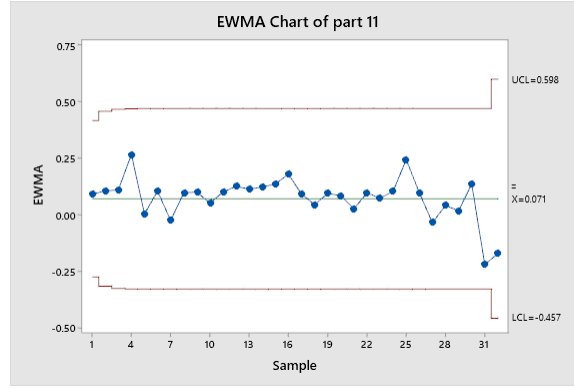


Figure 16 (c) EWMA control chart for layers 181-243 part 11

6. Conclusions and Future Research

This paper presents the modeling and monitoring framework on layer-wise images in 3D printing parts. An example of 16 basket samples shows the proposed methods are implemented to demonstrate the proposed framework can indeed be implemented for process monitoring based on a very limited number of parts printed. Two complimentary methods can successfully detect printing problems layer by layer. Some important findings of this study are as follows:

- EWMA control chart can be used for imaged based quality monitoring in addition to general purpose quality monitoring.
- A self-start charting method can be used after producing only two parts. In other words, process monitoring can start from the third part. The proposed method alleviates the need of the traditional control charting phase I requirement where at least 20 to 25 parts were recommended to establish control limits.
- Images quality and lightening issue was addressed by three machine learning techniques: Neural Network (NN), Gradient Boosting Classifier (GBC) and Support Vector Machine (SVM). GBC has the best performance in terms of accuracy and false identification rates.
- After printing enough part to have an accurate estimation of mean and standard deviation of the production, Method II using the cluster charting approach may be useful to reduce the charting overhead of the self-start charting approach from 243 charts to only three charts.

In the current study, we only need to know whether the printer is producing bad part or not and there is no need to find location of the issue. For future study, this method can be extended for a problem that needs to determine location of a problem. We will explore an approach to segment each image to smaller tiles and analyze those tiles. The problematic tile shows location of the issue as well. Also, if enough images are available, to determine whether a picture represent a good part or not, a deep learning algorithm may be used.

REFERENCES:

- Andres Patrignania, Tyson E. Ochsner. (2015). Canopeo: A Powerful New Tool for Measuring Fractional Green Canopy Cover . *Agronomy Journal*, 107(6), 2312-2320.
- Armingol, J. M., J. Otamendi, A. de la Escalera, J. M. Pastor, and F. J. Rodriguez. (2003). Statistical Pattern Modeling in Vision-based Quality Control Systems. *Journal of Intelligent and Robotic Systems*, 37(3), 321–336.
- B. C. Jiang, C.-C. Wang, H.-C. Liu. (2005). Liquid Crystal Display Surface Uniformity Defect Inspection Using Analysis of Variance and exponentially weighted moving average techniques. *International Journal of Production Research*, 43(1), 67-80.
- Bernard C. Jiang, S.J. Jiang. (1998). Machine vision based inspection of oil seals. *Journal of Manufacturing Systems*, 17(3), 159-166.
- Chee Kai Chua, Chee How Wong and Wai Yee Yeong. (2017). *Standards, quality control, and measurement sciences in 3d printing and additive manufacturing*. Matthew Deans.
- Elias NMalamas, Euripides G.M Petrakis, Michalis Zervakis, Laurent Petit, Jean-Didier Legat. (2003). A Survey on Industrial Vision Systems, Applications and Tools. *Image and Vision Computing*, 21(2), 171-188.
- Fadel M. Megahed, William H. Woodall & Jaime A. Camelio. (2011). A Review and Perspective on Control Charting with Image Data. *Journal of Quality Technology*, 43(2), 83-98.
- Farhad Imani , Bing Yao , Ruimin Chen , Prahalad Rao , Hui Yang. (2019). Joint Multifractal and Lacunarity Analysis of Image Profiles for Manufacturing Quality Control. *J. Manuf. Sci. Eng.*
- Farhad Imani, Aniruddha Gaikwad, Mohammad Montazeri, Prahalada Rao, Hui Yang, Edward Reutzel. (2018). Process Mapping and In-Process Monitoring of Porosity in Laser Powder Bed Fusion Using Layerwise Optical Imaging. *Journal of Manufacturing Science and Engineering*, 140.
- Farhad Imani, Ruimin Chen, Evan Diewald, Edward Reutzel, Hui Yang. (2019). Deep Learning of Variant Geometry in Layerwise Imaging Profiles for Additive Manufacturing Quality Control. *Journal of Manufacturing Science and Engineering*, 141.
- Hao Yan, Kamran Paynabar, and Jianjun Shi. (2015). Image-Based Process Monitoring Using Low-Rank Tensor Decomposition. *IEEE TRANSACTIONS ON AUTOMATION SCIENCE AND ENGINEERING*, 12(1), 216-227.
- HAWKINS, D. M. (1987). Self-starting cusum charts for location and scale . *The Statistician*, 299-315.
- Hsin-Chieh Wu, Tin-Chih Toly Chen. (2018). Quality control issues in 3D-printing manufacturing: a review. *Rapid Prototyping Journal*, 24(3), 607-615.
- ISO and ASTM. (2015). *ISO/ASTM 52900:2015 Additive manufacturing—General principles—Terminology*. ISO, ASTM International.
- Lin, H. D., and S. Chiu. (2006). Computer-aided Vision System for Mura-type Defect Inspection in Liquid Crystal Displays. *Lecture Notes in Computer Science*, 4319, 442–452.
- Ling Zuo, Zhen He, Min Zhang. (2019). An EWMA and region growing based control chart for monitoring image data. *QUALITY TECHNOLOGY & QUANTITATIVE MANAGEMENT*, 17(4), 470-485.
- Lu, C. J., and D. M. Tsai. (2005). Automatic Defect Inspection for LCDs Using Singular Value Decomposition. *The International Journal of Advanced Manufacturing Technology*, 25(1-2), 53–61.
- Megahed, F. M., L. J. Wells, J. A. Camelio, and W. H. Woodall. (2012). A Spatiotemporal Method for the Monitoring of Image Data. *Quality and Reliability Engineering International*, 28(8), 967–980.
- Mehdi Koosha, Rassoul Noorossana, Fadel Megahed. (2017). Statistical process monitoring via image data using wavelets. *Quality & Reliability Engineering International*, 33, 2059–2073.
- Mohammadhossein Amini, Shing I.Chang. (2018). MLCPM: A process monitoring framework for 3D metal printing in industrial scale. *Computers & Industrial Engineering*, 322-330.
- Montgomery, D. C. (2013). *Statistical Quality Control*. John Wiley & Sons, Inc.
- R.L. Horst, M. Negin. (1992). Vision system for high-resolution dimensional measurements and on-line SPC: web process application. *IEEE Transactions on Industry Applications*, 28(4), 993 - 997 .
- SASAM. (2015). *Additive manufacturing: SASAM standardisation roadmap*. SASAM.
- Shing I.Chang, Behnam Tavakkol, Shih-Hsiung Chou, Tzong-Ru Tsai. (2014). Real-time detection of wave profile changes. *Computers & Industrial Engineering*, 75, 187-199.
- Sullivan, J. H. (2002). Detection of Multiple Change Points from Clustering Individual Observations. *Journal of Quality Technology*, 34(4), 371-383.
- Tunák, M., and A. Linka. (2008). Directional Defects in Fabrics. *Research Journal of Textile and Apparel*, 12(2), 13–22.
- Ugandhar Delli, Shing Chang. (2018). Automated Process Monitoring in 3D Printing Using Supervised Machine Learning. *Procedia Manufacturing*, 26, 865-870.
- Wang, K., and F. Tsung. (2005). Using Profile Monitoring Techniques for a Data-rich Environment with Huge Sample Size. *Quality and Reliability Engineering International*, 21(7), 677–688.

- Xiaoxiao Guo, Z. H. (2019). A Real-Time Contrasts Method for Monitoring Image Data. *IEEE 6th International Conference on Industrial Engineering and Applications*. Tokyo, Japan.
- Zhen He, Ling Zuo, Min Zhanga, Fadel M. Megahed. (2016). An image-based multivariate generalized likelihood ratio control chart for detecting and diagnosing multiple faults in manufactured products. *International Journal of Production Research*, 54(6), 1771-1784.